Perovskite Solar Cells Hot Paper

DOI: 10.1002/ange.201405176

High-Performance Hole-Extraction Layer of Sol–Gel-Processed NiO Nanocrystals for Inverted Planar Perovskite Solar Cells**

*Zonglong Zhu, Yang Bai, Teng Zhang, Zhike Liu, Xia Long, Zhanhua Wei, Zilong Wang, Lixia Zhang, Jiannong Wang, Feng Yan, and Shihe Yang**

Abstract: *Hybrid organic/inorganic perovskite solar cells have been rapidly evolving with spectacular successes in both nanostructured and thin-film versions. Herein, we report the use of a simple sol–gel-processed NiO nanocrystal (NC) layer as the hole-transport layer in an inverted perovskite solar cell. The thin NiO NC film with a faceted and corrugated surface enabled the formation of a continuous and compact layer of well-crystallized $CH_3NH_3PbI_3$ in a two-step solution process. The hole-extraction and -transport capabilities of this film interfaced with the $CH_3NH_3PbI_3$ film were higher than those of organic PEDOT:PSS layers. The cell with a NiO NC film with a thickness of 30–40 nm exhibited the best performance, as a thinner layer led to a higher leakage current, whereas a thicker layer resulted in a higher series resistance. With the NiO film, we observed a cell efficiency of 9.11 %, which is by far the highest reported for planar perovskite solar cells based on an inorganic hole-extracting layer.*

Hybrid organic/inorganic perovskite materials are currently among the most competitive absorbers for efficient solar cells.[1] Since they were first reported, perovskite-based solar cells have reached an efficiency of almost 16 %,[2] owing to the advantageous characteristics of perovskite materials: an appropriate direct band gap, a high absorption coefficient, and a propensity to form thin films with excellent carrier-transport properties and an apparent tolerance of defects.[3] The design versatility of perovskite solar cells has allowed either a mesoporous metal-oxide scaffold or simply a thin-film structure to be adopted, both with high efficiency over 15 %.[4] However, in all these high-efficiency cells, costly spiro-OMeTAD is used for the hole-transport layer, which hampers the commercialization of perovskite solar cells.[5] Recently, an inverted thin-film perovskite solar cell was reported in which the perovskite layer was sandwiched between a planar layer of the electron acceptor and the transparent hole acceptor poly(3,4-ethylenedioxythiophene):polystyrene sulfonate (PEDOT:PSS), which is widely used in organic photovoltaic devices.[6] However, PEDOT:PSS is less than ideal owing to its acidity, tendency to absorb water, and inability to block electrons.[7] A tantalizing possibility is to use p-type inorganic materials (NiO, CuSCN, etc.) to replace the PEDOT:PSS layer.[8] A salient problem with the use of a NiO hole-transport layer in perovskite solar cells is the difficulty for it to support a sufficiently thick perovskite film (typically < 60 nm), which has so far limited the cell efficiency.[9] Thus, elaboration of the NiO layer is required to enhance its anchoring capability. An ideal p-NiO film for high photovoltaic (PV) performance should 1) have good optical transparency, 2) prevent electron leakage, 3) have appropriate energy levels, and 4) support a high-quality and sufficiently thick perovskite film.[10] The last point is of particular interest and constitutes the theme of the present study.

We synthesized a layer of well-joined nickel oxide nanocrystals (NCs) for hole extraction and transport, each with a size of 10–20 nm, on fluorine-doped tin oxide (FTO) substrates. This NiO NC layer exhibited a higher transparency than that of conventional NiO thin films, thus saving the incident light for the active absorber. Also controlled aggregation of the faceted NiO nanocrystals resulted in a corrugated surface that could support an approximately 300 nm thick film of cubic $CH_3NH_3PbI_3$ crystals with good coverage and interconnectivity. These advantageous features of the NiO NC layer led to a high efficiency of the inverted perovskite solar cells of over 9.11 %. Photoluminescence (PL) studies revealed a higher hole-extraction ability of the NiO NC layer than those of PEDOT:PSS and NiO thin films.

We used atomic force microscopy (AFM) and transmission electron microscopy (TEM) to characterize the morphology of the NiO NC films. The AFM image in Figure 1 A shows that high-quality NiO nanocrystals with a size of 10–20 nm were uniformly deposited and well-connected after spin coating and annealing of the sol–gel precursor. For a typical synthesis of the NiO NC film, the sol solution was prepared by dissolving nickel(II) acetylacetonate in diethanolamine. The precursor was heated at 150 °C to form the sol suspension, which was then spin coated on to the FTO, followed by annealing at 500 °C. Figure 1 B shows the

[*] Z. L. Zhu,[+] T. Zhang, Prof. S. H. Yang
Nano Science and Technology Program
The Hong Kong University of Science and Technology
Clear Water Bay, Kowloon, Hong Kong (China)
E-mail: chsyang@ust.hk
Z. L. Zhu,[+] Y. Bai,[+] T. Zhang, Dr. X. Long, Z. H. Wei, Z. L. Wang, Prof. S. H. Yang
Department of Chemistry
The Hong Kong University of Science and Technology
L. X. Zhang, Prof. J. N. Wang
Department of Physics
The Hong Kong University of Science and Technology
Dr. Z. K. Liu, Prof. F. Yan
Department of Applied Physics and Materials Research Centre
The Hong Kong Polytechnic University, Hong Kong (China)
[+] These authors contributed equally.

[**] This research was supported by the HK-RGC General Research Funds (HKUST 606511 and 605710).
Supporting information for this article is available on the WWW under http://dx.doi.org/10.1002/anie.201405176.

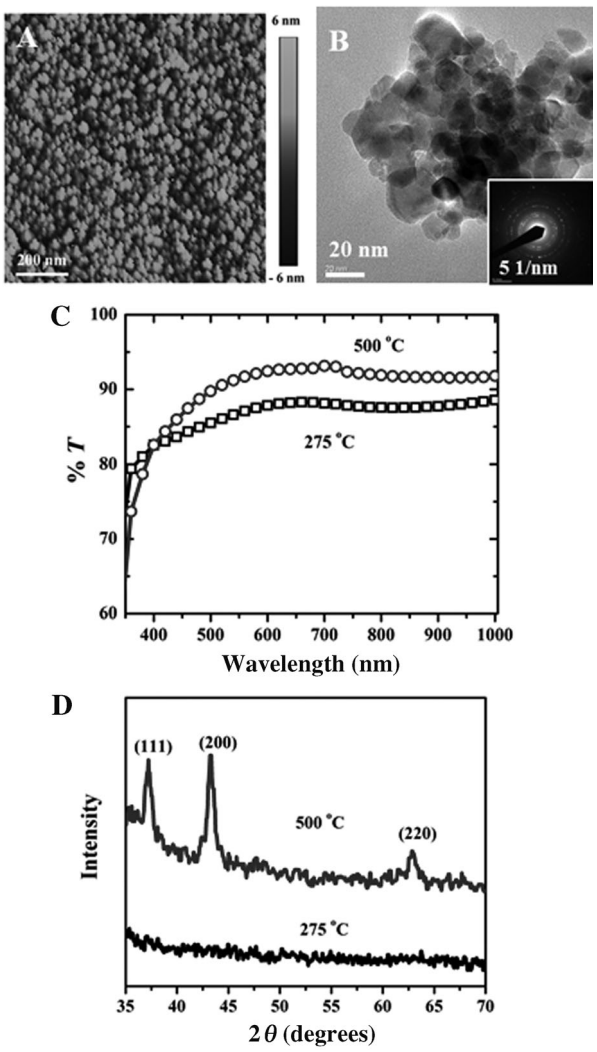

Figure 1. A) AFM roughness image of a NiO nanocrystal film on FTO. B) Bright-field TEM image of a sample of NiO NCs with the corresponding diffraction pattern (inset). C) Optical transmission spectra and D) XRD patterns of NiO NC films grown on quartz and annealed at different temperatures.

TFM image, which confirms the size of the NiO nanocrystals at 10–20 nm. As a result of the heating process, the NiO NCs aggregated together and became well-connected, which was expected to be beneficial for hole transfer through the NiO film. The electron-diffraction pattern (inset in Figure 1B) shows a polycrystalline NiO structure, and from a high-resolution TEM (HRTEM) image (see Figure S1 in the Supporting Information), the outer d spacing of the nanocrystals was measured to be 0.21 nm, which matches well with the interplanar spacing of (200). We determined the optical properties as well as the crystal and electronic structures of the thin films (Figure 1C,D). First of all, our NiO NC film (500 °C) showed higher transparency than the low-temperature NiO film (275 °C; Figure 1C), which is highly desirable for solar-cell devices because it preserves the incoming photons for the neighboring absorber layer. The higher transparency of our NiO NC film (500 °C) is clearly due to the annealing-induced crystallization, which eliminates defect states and impurities. Indeed, the low-temperature NiO film did not exhibit any X-ray diffraction (XRD) peaks (Figure 1D), thus indicating that the NiO is either amorphous or too weakly crystalline. In contrast, for the NiO NC film, several clear peaks belonging to the cubic NiO crystal structure in the space group *Fm3m* (NaCl-type) were observed, including (111), (200), and (220).

Ultraviolet photoelectron spectroscopy (UPS) was used to probe the work functions (Φ) of the NiO thin film,[11] the NiO NC layer, and the PEDOT:PSS film (Figure 2A,B; see Figure S2 for the full UPS spectra). The Φ value of the NiO NC layer was 5.36 eV, thus indicating that the electron-donor level of NiO NC layer matches well with the energy level of the valence-band (VB) edge (−5.4 eV) of $CH_3NH_3PbI_3$ for facile hole extraction. However, the Φ values of the NiO thin film (5.12 eV) and the PEDOT:PSS film (5.21 eV) are both higher than the VB edge of $CH_3NH_3PbI_3$: a situation unfavorable for hole extraction. The appropriate energy-level alignment with the NiO NC layer bodes well for the performance of the corresponding solar-cell devices.

We further studied the NiO NCs and NiO thin film by X-ray photoelectron spectroscopy (XPS) to gain information about their structure and composition.[12] Figure 2C,E shows the Ni $2p_{3/2}$ XPS spectra. The first of the two common peaks observed, the left peak at the binding energy of 861.3 eV, is ascribed to a shakeup process in the NiO structure, and the second, right peak at 855.5 eV is due to the Ni^{2+}-vacancy-induced Ni^{3+} ion or nickel hydroxides ($Ni^{II}OH$) and oxyhydroxides ($Ni^{III}OOH$). However, there is an additional intense peak at 853.7 eV for the NiO NC film. This peak corresponds to the Ni^{2+} in the standard Ni–O octahedral bonding configuration in cubic rock-salt NiO. This assignment was verified by the O 1s XPS spectra in Figure 2D,F. Although the peaks of NiOOH (531.9 eV) and NiO (529.2 eV) appear in both samples, the huge difference in the intensity ratio of the peaks indicates that the NiO thin film has not been completely transformed from the precursor into well-crystallized NiO. Thus, the XPS results proved that our NiO NC film chiefly adopts the Ni–O octahedral bonding configuration, whereas in the NiO thin film, there exists a large amount of $Ni^{II}O$ and $Ni^{III}OOH$ owing to the low-temperature process.

The relevant energy levels for the solar-cell device, including the valence-band (VB) and conduction-band (CB) edges of each layer, are shown in Figure 3A. On light absorption, excitons are generated in the $CH_3NH_3PbI_3$ layer and then dissociated, followed by transfer of the electron to the phenyl-C_{61}-butyric acid methyl ester (PCBM) layer and the hole to the NiO layer. For the cubic structure of NiO shown in Figure 3B, the VB edge (−5.5 eV) of NiO is very close to the VB edge of $CH_3NH_3PbI_3$ (−5.4 eV), and the Fermi level (E_f) of the NiO NCs is even higher (−5.36 eV), thus making hole extraction favorable from $CH_3NH_3PbI_3$ to NiO NCs.

Figure 3C shows the cross-sectional-view SEM image of a glass/FTO/NiO/$CH_3NH_3PbI_3$ film. To prepare this film, we applied the two-step $CH_3NH_3PbI_3$-deposition method of Grätzel and co-workers.[4b,13] The $CH_3NH_3PbI_3$ perovskite layer can be readily distinguished with a thickness of 250 nm, and the layer of NiO NCs has a thickness of about 40 nm. The

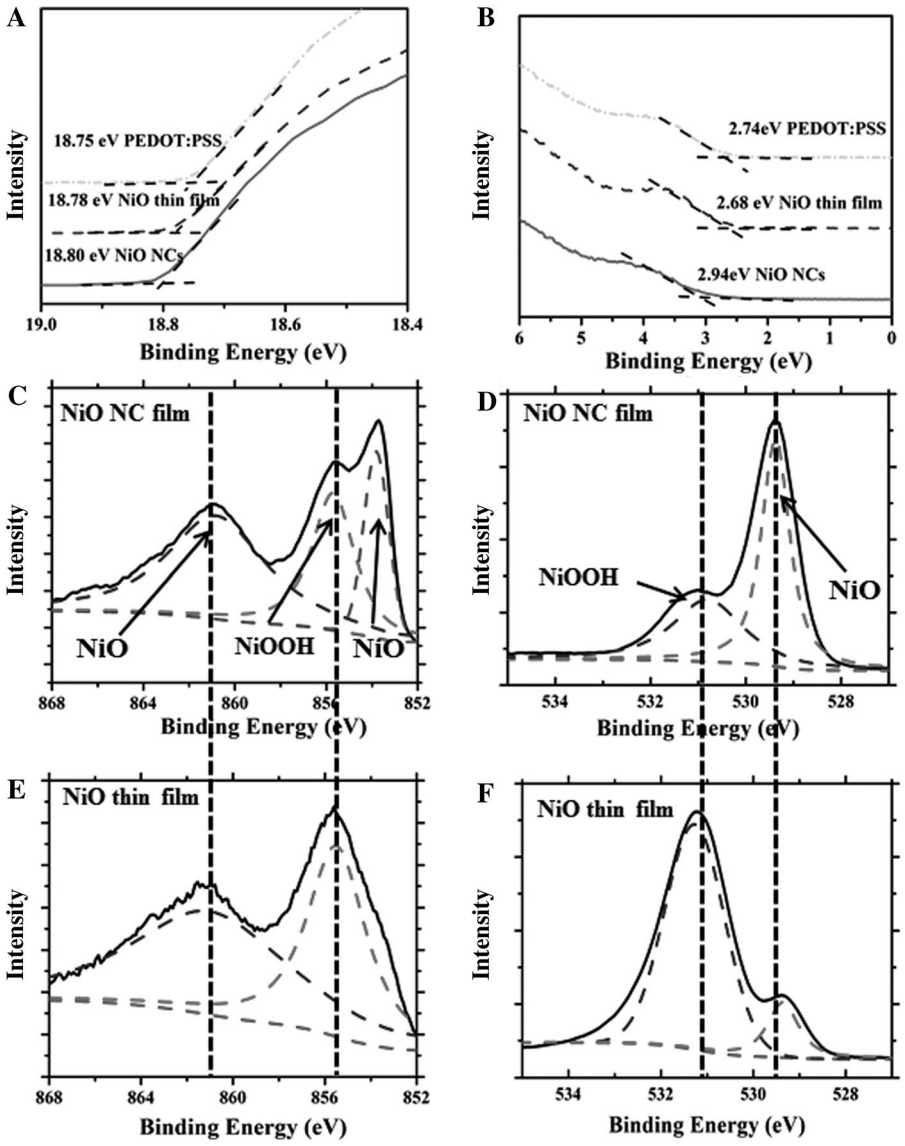

Figure 2. Photoelectron spectroscopy of the various films studied. A,B) UPS spectra (He I radiation <) of the NiO NCs, the NiO thin film, and PEDOT:PSS in the cutoff (A) and onset regions (B). C–F) XPS spectra at the Ni $2p_{3/2}$ and O 1s core levels of a NiO NC film (C,D) and a NiO thin film (E,F).

top-view image (Figure 3D) shows that a well-crystallized cubic phase of the $CH_3NH_3PbI_3$ perovskite layer was formed on top of the layer of NiO NCs. For comparison, top-view and cross-sectional images (see Figure S4) of $CH_3NH_3PbI_3$ on PEDOT:PSS and on a NiO thin-film layer formed by low-temperature solution processing showed no clear cubic phase of $CH_3NH_3PbI_3$ deposited on PEDOT:PSS and inadequate coverage of perovskite on the polymer surface, although the films were formed by the same two-step deposition method. It is possible that the *N*,*N*-dimethylformamide and isopropanol would dissolve part of the PEDOT:PSS during spin coating of the PbI_2 precursor and dip coating in CH_3NH_3I solution. Similarly, the SEM images of the low-temperature NiO thin-film/perovskite composite (see Figure S4C,D) explain why these films also show lower cell performance than the NiO NC layer, as described in more detail below. To put it simply, because of the smoother surface of the low-temperature NiO thin films, the coverage of $CH_3NH_3PbI_3$ is much poorer than on the layer of NiO NCs, and there are bare areas without any perovskite coating. Comparison of the cross-sectional-view images between Figure 3C and Figure S4D (see the Supporting Information) shows that a thicker layer of closely joined, larger cubic $CH_3NH_3PbI_3$ crystals could be formed on the NiO NC layer. Clearly, the roughness of the surface of the NiO film plays a large role in directing the overgrowth of the perovskite layer, especially for two-step deposition. Understandably, the roughness causes PbI_2 to be deposited in a relatively thick and well-connected layer by high-speed spin coating. Owing to this well-crystallized, interconnected, and thick $CH_3NH_3PbI_3$ layer, our perovskite solar cell based on a NiO NC layer could deliver higher efficiency, as a result of a higher photocurrent and voltage, as discussed in more detail below.

Typical curves of photocurrent density (J) versus voltage (V) for solar cells with different NiO films are shown in Figure 4A, and the parameters for PV performance are summarized in Table 1. To examine the thickness effect, we fabricated a series of perovskite solar cells with NiO NC layers of different thicknesses. The champion turned out to be the perovskite solar cell with a NiO NC layer with a thickness of 40 nm. This solar cell exhibited the highest power-conversion efficiency (PCE) of 9.11%, with a short-circuit current (J_{sc}) of 16.27 mA cm^{-2}, an open-circuit voltage (V_{oc}) of 0.882 V, and a fill factor (FF) of 0.635. The perovskite solar cell with a 20 nm layer of NiO NCs showed a PCE value of 6.04% with $J_{sc} = 13.64$ mA cm^{-2}, $V_{oc} = 0.704$ V, and $FF = 0.630$, and the perovskite solar cell with a 70 nm NiO NC layer showed a PCE value of 5.58% with $J_{sc} = 10.72$ mA cm^{-2}, $V_{oc} = 0.851$ V, and $FF = 0.612$. The performance of the PEDOT:PSS-based perovskite solar cell is also plotted in Figure 4. We found that at a 40 nm thickness of the NiO NC layer, the V_{oc} and J_{sc} values were highest. The improvement in V_{oc} and J_{sc} in going from the 20 nm to the 40 nm film is ascribed to the improved electron blocking and the reduced charge recombination and leakage current, as observed previously by other research groups.[14] On the other hand, for the film-thickness increase from 40 to 70 nm, the decrease in photocurrent and voltage is most likely due to the increased series resistance and photoabsorption of the NiO_x NC film.[15]

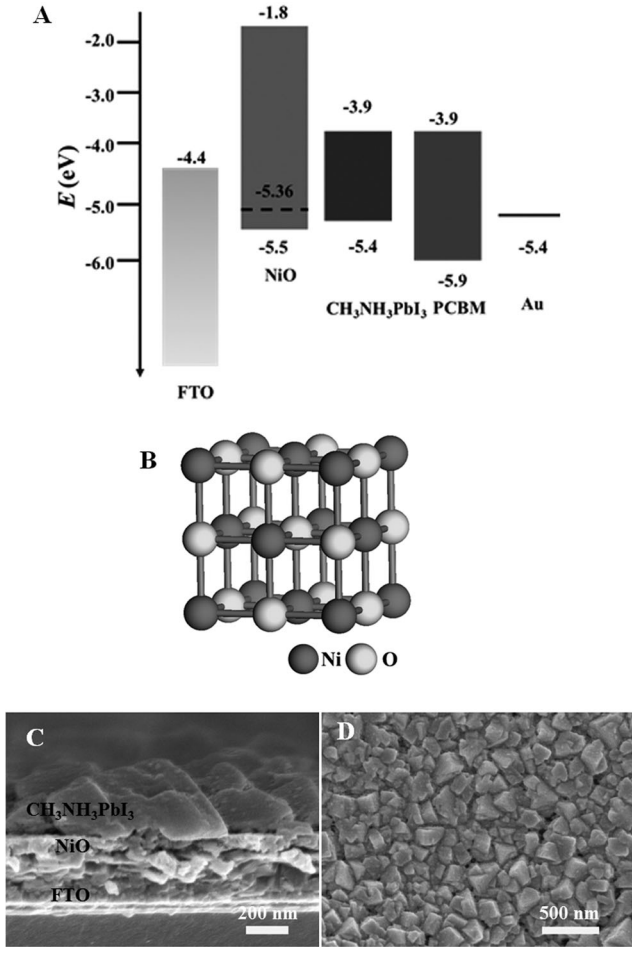

Figure 3. A) Energy-level-alignment diagram of the device components (relative to the vacuum level). The dashed line shows the Fermi level of NiO NCs from the UPS measurement. B) Crystal structure of NiO. C) Cross-sectional-view and D) top-view SEM images of a typical device based on the glass/FTO/NiO/$CH_3NH_3PbI_3$ structure.

In comparison, the performance of the perovskite solar cells based on the low-temperature NiO thin film and PEDOT:PSS was generally low. The very low V_{oc} (0.647 V) and J_{sc} values (9.82 mA cm^{-2}) for the cell based on the NiO thin film can be explained by the following factors: 1) the higher work function, as discussed above along with the UPS results, 2) the poorly crystallized and interconnected $CH_3NH_3PbI_3$ particles, and 3) the insufficient thickness of the absorber layer. For the PEDOT:PSS-based cell, on the other hand, the very large bare area not covered by $CH_3NH_3PbI_3$ appears to be the main reason for the low efficiency. We also examined the incident-photon-to-current efficiency (IPCE; Figure 4B). The integrated photocurrent from the IPCE is consistent with the measured J_{sc} value. We note that the IPCE is similar to those reported previously by others for inverted perovskite solar cells, and the small dip at 650 nm could result from reduced absorption of the perovskite.[16]

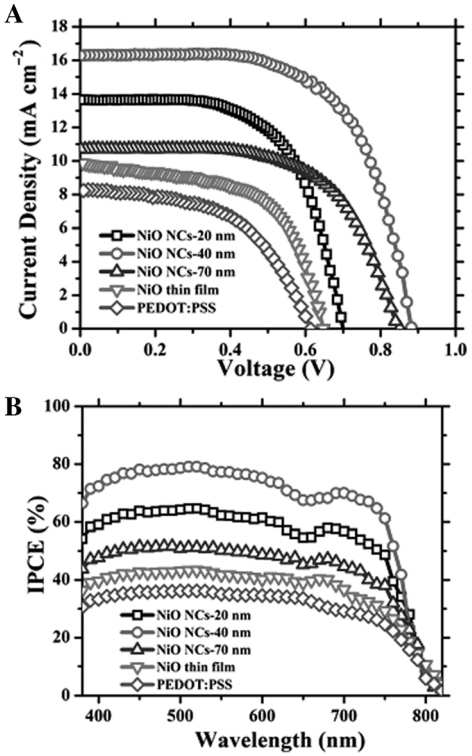

Figure 4. Typical *J*–*V* curves and IPCE spectra of the perovskite solar cells. A) Photocurrent density versus applied voltage. B) IPCE spectra of perovskite solar cells with different NiO hole-transport layers and PEDOT:PSS.

We performed steady-state photoluminescence (PL) and time-resolved photoluminescence (TRPL) measurements to study exciton diffusion in the hole-transport layers. The normalized steady-state PL spectra in Figure 5A show that the PL quenching with the NiO NCs is the most dramatic among all of the samples. This result shows that the NiO NC layer is the most effective hole extractor owing to the high interfacial film quality with intimate contact with the perovskite and the high mobility. The TRPL profiles in Figure 5B show that the PL decay rate is also highest for the NiO NC layer. We fitted the PL decay curve to a biexponential function [Eq. (1); see the Supporting Information for the fitting result].

$$I(t) = A_1 \exp\left(\frac{t}{\tau_1}\right) + A_2 \exp\left(\frac{t}{\tau_2}\right) \quad (1)$$

Typically, the initially photogenerated excitons diffuse into defects, and the small time constant τ_1 reflects this early event. It is the large time constant τ_2 that is associated with the

Table 1: Parameters for the photovoltaic devices with different transport layers.

NiO thickness (device)	V_{OC} [V]	J_{SC} [mA cm^{-2}]	*FF*	PCE [%]	R_s [Ω cm^{-2}]	Work function [eV]
20 nm (NCs)	0.704	13.64	0.630	6.04	12.6	5.36
40 nm (NCs)	0.882	16.27	0.635	9.11	17.4	5.36
70 nm (NCs)	0.851	10.72	0.612	5.58	22.8	5.36
40 nm (thin film)	0.647	9.82	0.591	3.75	21.6	5.12
PEDOT:PSS	0.613	8.25	0.533	2.70	24.1	5.21

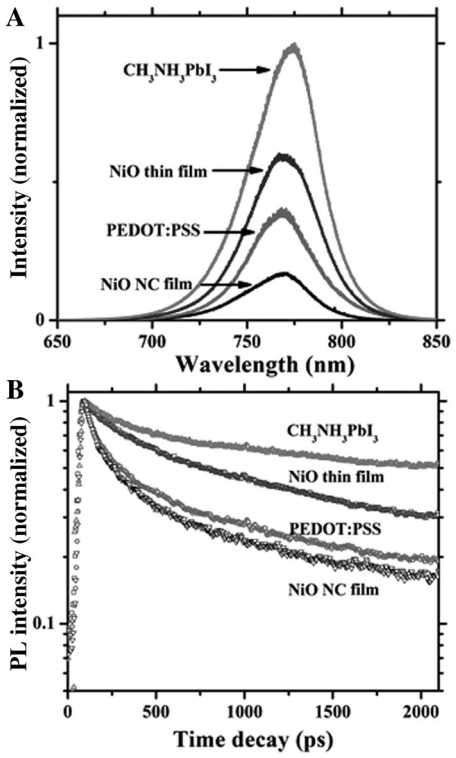

Figure 5. A) Steady-state PL spectra (excitation at 514.5 nm (20 mW)) and B) transient PL decay (excitation at 400 nm (1 $W cm^{-2}$)) of NiO NCs (40 nm), PEDOT:PSS, and a NiO thin film interfaced with a $CH_3NH_3PbI_3$ film. The bare $CH_3NH_3PbI_3$ film was used as a reference.

exciton lifetime of $CH_3NH_3PbI_3$. Thus, a small τ_2 value will indicate a fast exciton- or hole-diffusion process. Indeed, of all the samples we studied, our NiO NC layer exhibited the smallest τ_2 value, which corresponds to the highest hole-extraction and -transport efficiency. These high hole-extraction and -transport rates contribute significantly to the high J_{sc} value for the perovskite solar cell with a NiO NC layer.

In conclusion, we have used a sol–gel process to fabricate a thin NiO nanocrystalline film for the development of a NiO/$CH_3NH_3PbI_3$ solar-cell device. A key finding is that the rough NiO film surface formed by the aggregation of faceted NiO nanoscale monocrystals permits the formation of an intimate, large interfacial-area junction with the $CH_3NH_3PbI_3$ film, thereby dramatically enhancing the cell efficiency. More specifically, the rough NiO surface is beneficial for the deposition of PbI_2 in the first step, and during the dipping process, $CH_3NH_3PbI_3$ experiences unconstrained crystallite growth that occurs in the absence of a mesoporous scaffold. Large crystallites of $CH_3NH_3PbI_3$ accrete as guided by the rough NiO surface, thus leading to a highly textured $CH_3NH_3PbI_3$/PCBM interface with dimensions commensurate with the electron–hole diffusion lengths. The crystallites also act as efficient light-scattering centers, which increase the effective optical path length of the device. The combination of these effects as well as the suitable energy levels of the NiO NC layer yielded a PCE of up to 9.11%, which, to our knowledge, is the highest reported for inverted planar $CH_3NH_3PbI_3$ solar-cell devices with an inorganic hole transporter. Thus, this study has demonstrated a simple and readily processable perovskite solar cell based on a NiO nanocrystal hole-extraction layer with an inverted planar structure rather than a mesoporous structure. It opens the way for the design of hybrid tandem solar cells, in which other layers could be made, for example, on the basis of existing copper indium sulfide or c-Si technologies.

Received: May 11, 2014
Published online: July 15, 2014

Keywords: energy conversion · inorganic hole-extraction layers · NiO nanocrystals · organic–inorganic hybrid composites · perovskite solar cells

[1] a) M. D. McGehee, *Nature* **2013**, *501*, 323–325; b) G. Hodes, *Science* **2013**, *342*, 317–318; c) Z. Zhu, J. Ma, Z. Wang, C. Mu, Z. Fan, L. Du, Y. Bai, L. Fan, H. Yan, D. L. Phillips, S. Yang, *J. Am. Chem. Soc.* **2014**, *136*, 3760–3376.
[2] K. Wojciechowski, M. Saliba, T. Leijtens, A. Abate, H. J. Snaith, *Energy Environ. Sci.* **2014**, *7*, 1142–1147.
[3] a) Q. Chen, H. P. Zhou, Z. R. Hong, S. Luo, H. S. Duan, H. H. Wang, Y. S. Liu, G. Li, Y. Yang, *J. Am. Chem. Soc.* **2014**, *136*, 622–625; b) H. J. Snaith, *J. Phys. Chem. Lett.* **2013**, *4*, 3623–3630; c) H.-S. Kim, S. H. Im, N.-G. Park, *J. Phys. Chem. C* **2014**, *118*, 5615–5625.
[4] a) M. Liu, M. B. Johnston, H. J. Snaith, *Nature* **2013**, *501*, 395–398; b) J. Burschka, N. Pellet, S.-J. Moon, R. Humphry-Baker, P. Gao, M. K. Nazeeruddin, M. Grätzel, *Nature* **2013**, *499*, 316–319.
[5] N. G. Park, *J. Phys. Chem. Lett.* **2013**, *4*, 2423–2429.
[6] a) P. Docampo, J. M. Ball, M. Darwich, G. E. Eperon, H. J. Snaith, *Nat. Commun.* **2013**, *4*, 2761; b) O. Malinkiewicz, A. Yella, Y. H. Lee, G. Mínguez Espallargas, M. Graetzel, M. K. Nazeeruddin, H. J. Bolink, *Nat. Photonics* **2014**, *8*, 128–132.
[7] J. R. Manders, S. W. Tsang, M. J. Hartel, T. H. Lai, S. Chen, C. M. Amb, J. R. Reynolds, F. So, *Adv. Funct. Mater.* **2013**, *23*, 2993–3001.
[8] a) K. X. Steirer, P. F. Ndione, N. E. Widjonarko, M. T. Lloyd, J. Meyer, E. L. Ratcliff, A. Kahn, N. R. Armstrong, C. J. Curtis, D. S. Ginley, J. J. Berry, D. C. Olson, *Adv. Energy Mater.* **2011**, *1*, 813–820; b) P. Qin, S. Tanaka, S. Ito, N. Tetreault, K. Manabe, H. Nishino, M. K. Nazeeruddin, M. Graetzel, *Nat. Commun.* **2014**, *5*, 3834.
[9] a) J. Y. Jeng, K.-C. Chen, T. Y. Chiang, P. Y. Lin, T. D. Tsai, Y. C. Chang, T. F. Guo, P. Chen, T. C. Wen, Y.-J. Hsu, *Adv. Mater.* **2014**, *26*, 4107–4113; b) H. Tian, B. Xu, H. Chen, E. M. J. Johansson, G. Boschloo, *ChemSusChem.* **2014**, DOI: 10.1002/cssc.201402032.
[10] M. D. Irwin, B. Buchholz, A. W. Hains, R. P. H. Chang, T. J. Marks, *Proc. Natl. Acad. Sci. USA* **2008**, *105*, 2783–2787.
[11] Y. Park, V. Choong, Y. Gao, B. R. Hsieh, C. W. Tang, *Appl. Phys. Lett.* **1996**, *68*, 2699–2701.
[12] E. L. Ratcliff, J. Meyer, K. X. Steirer, A. Garcia, J. J. Berry, D. S. Ginley, D. C. Olson, A. Kahn, N. R. Armstrong, *Chem. Mater.* **2011**, *23*, 4988–5000.
[13] D. Liu, T. L. Kelly, *Nat. Photonics* **2014**, *8*, 133–138.
[14] a) J. Kettle, H. Waters, M. Horie, S. W. Chang, *J. Phys. D* **2012**, *45*, 125102; b) H. Yang, C. Gong, G. H. Guai, C. M. Li, *Sol. Energy Mater. Sol. Cells* **2012**, *101*, 256–261.
[15] Z. C. Zhai, X. D. Huang, M. F. Xu, J. Y. Yuan, J. Peng, W. L. Ma, *Adv. Energy Mater.* **2013**, *3*, 1614–1622.
[16] J. B. You, Z. R. Hong, Y. Yang, Q. Chen, M. Cai, T. B. Song, C. C. Chen, S. R. Lu, Y. S. Liu, H. P. Zhou, Y. Yang, *Acs Nano* **2014**, *8*, 1674–1680.

